Performance of CdZnTe Geometrically Weighted Semiconductor Frisch Grid Radiation Detectors

D.S. McGregor[1] and R.A. Rojeski[2]
[1]Department of Nuclear Engineering and Radiological Sciences, University of Michigan, MI 48109-2104
[2]Etec Systems, Inc., 26460 Corporate Ave., Hayward, CA 94545

Abstract

Semiconductor Frisch grid radiation detectors have been manufactured and tested with encouraging results. Resolution enhancement occurs as a result of combining the geometric weighting effect, the "small pixel" effect and the Frisch grid effect. The devices are operated at ambient temperature without any pulse shape correction, rejection and compensation techniques. The new devices are manufactured from CdZnTe and do not require any cooling for operation. The geometrically weighted detectors have only one signal output to a standard commercially available Ortec 142A preamplifier. The detectors operate with simple commercially available NIM electronics, hence the device design can be coupled to any typical NIM system without the need for special electronic instruments or circuits. Geometrically weighted detectors that are 1 cubic centimeter in volume were fabricated from "counter grade" material, yet have shown room temperature energy resolution of 7.5% FWHM (at 29°C) for ^{57}Co 122 keV gamma rays and 2.68% FWHM (at 23°C) for ^{137}Cs 662 keV gamma rays.

I. Introduction

Wide bandgap compound semiconductors offer promise as potential room temperature operated radiation spectrometers [1-3]. General realization of compound semiconductors as practical and efficient radiation spectroscopy devices has been inhibited by material problems, the most severe being charge carrier trapping [4,5]. Charge carrier trapping effects can be reduced by confining the devices to small volumes [5], and relatively small devices have demonstrated impressive energy resolution at the expense of reasonable gamma ray interaction efficiency [3]. In some cases, devices that yield good energy resolution at room temperature are most important, and tiny wide bandgap semiconductor detectors may be adequate. However, efficient spectra for moderately high energy gamma rays require large volume detectors fabricated from reasonably large atomic number materials. Quite often small room temperature compound semiconductor devices seem less attractive than scintillation based detectors and hand held portable high purity germanium (HPGe) detectors.

For most compound semiconductors, the "hole" charge carrier drift mobility (μ_h) in the valence band is significantly less than the electron charge carrier drift mobility (μ_e) in the conduction band. Additionally, it is generally true that the mean free drift time for holes (τ^*_h) is shorter than the mean free drift time for electrons (τ^*_e). The effect of the lower μ_h and τ^*_h values combine such that hole charge carrier losses limit the achievable resolution for planar geometry compound semiconductor radiation spectrometers.

Methods of compensating hole trapping losses have been demonstrated, including electronic pulse height discrimination and correction [6-8], and single polarity sensing devices [9-17]. Electronic correction generally consists of added circuitry capable of discriminating between pulses that demonstrate severe "hole" trapping and those dominated by electron transport, in which case the poor signal is either discriminated out [6,7] or the signal is corrected to the expected value [7,8]. Early single polarity devices were geometrically weighted (such as spherical devices) to enhance induced charge signal contributions from electron motion while minimizing induced charge signal contributions from hole motion, thereby minimizing the effect of hole charge carrier trapping [9,10]. More recent single polarity devices utilize the Frisch grid concept [18-20] to screen out and reduce the effects of hole trapping. Such configurations include co-planar designs [11-13], drift detector designs [14,15] and Frisch grid designs [16,17]. All of the mentioned methods have shown promise and detectors implementing the techniques and designs have demonstrated good room temperature gamma ray energy resolution. Drawbacks to these designs include manufacturing difficulties and relatively complex electronics. Recently the authors introduced a very simple device that utilizes the geometrical weighting concept coupled with the Frisch grid concept [21]. The new design demonstrates good single polarity sensitivity and requires only one commercially available preamplifier for the output. Included in the present work are theoretical considerations compared to the experimental performance of such devices.

II. Theoretical Considerations and Detector Design

The fundamental treatment for induced charge pulses measured from a planar semiconductor radiation detector can be found in the literature [4,5,22,23]. With the assumption that gamma ray interactions are uniform, the measured induced charge (Q^*) as a function of photoelectric gamma ray interaction location can be estimated from the Hecht relation

$$Q^* = Q_o\{\rho_e(1-\exp[(x_i - W_D)/\rho_e W_D]) + \rho_h(1-\exp[-x_i/\rho_h W_D])\} \quad , \qquad (1)$$

where Q_o is the initial charge excited by the interacting gamma ray, W_D is the detector length, x_i represents the interaction location in the detector as measured from the cathode, and ρ is the *carrier extraction factor* (CEF) represented by

0018-9499/99$10.00

$$\rho_{e,h} = \frac{v_{e,h}\,\tau^{*}_{e,h}}{W_D} \quad , \qquad (2)$$

where v is the charge carrier velocity and τ^* is the carrier mean free drift time, and the e and h subscripts refer to electrons or holes, respectively. It can be shown from equations 1 and 2 that energy resolution will degrade if the either carrier extraction factor is reduced significantly below 50 [see ref. 5]. The worst cases appear when one value of ρ is not only significantly less than 50, but also quite different than the other CEF. Hence, the charge carrier type with the *worst* transport properties (generally holes) determines the spectral response. Since charge carrier velocities are saturation limited [24] and the mean free drift times are also material related, the values for ρ are most commonly increased by reducing W_p. Clearly the method limits gamma ray interaction efficiency.

Parallelepiped style semiconductor Frisch grid detectors [16,17] provide a simple method to isolate electron induced charge signals from hole induced charge signals. The basic device has three distinctive regions: (1) the interaction region where most gamma rays interact, (2) the pervious region where charge carriers pass through the Frisch grid, and (3) the measurement region where the induced charge is measured as carriers move between the Frisch grid and the anode. Spectroscopic performance is primarily determined by the charge carrier type with the *best* transport properties (generally electrons). Two significant drawbacks limit the performance of the parallelepiped semiconductor Frisch grid detectors: (1) the devices are relatively thin to preserve the screening action of the Frisch grid and (2) the resulting gamma ray spectra has significant hole trapping "contamination" from gamma ray interactions in the measurement region [17].

The geometrically weighted design improves the performance of semiconductor Frisch grid detectors. Figure 1 shows the basic features of a geometrically weighted semiconductor Frisch grid radiation detector. The device dimensions are designated as follows: cathode width = W_c, anode width = W_a, width at the pervious region center = W_p, interaction region height = L_i, pervious region height = L_p, measurement region height = L_m, overall detector height = H and the detector depth = D. The unique geometrical shape and electrode configuration provide several effects that work together to improve energy resolution. Among these effects are the geometric weighting effect, the small pixel effect and the Frisch grid effect.

A. *The Geometric Weighting Effect*

1. The Case of Uniform Irradiation

Consider the geometric shape of a trapezoid prism detector. For simplicity, let us assume that gamma ray interactions occur uniformly throughout the detecting volume. We also assume that photoelectric absorption is dominant within the detector (no Compton scattering and no pair production). Hence, the gamma ray interaction rate is

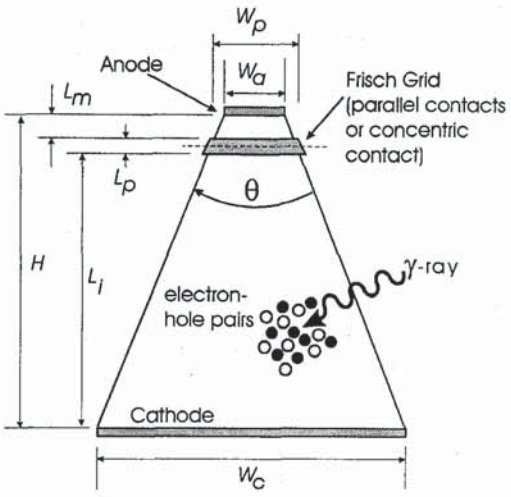

Figure 1. Diagram showing the general features for a geometrically weighted semiconductor Frisch grid radiation spectrometer.

uniform and constant for any unit volume *dxdydz* within the detector. Indeed the case is unrealistic, yet it will serve to clarify the advantage of the geometric weighting effect. The overall volume of the device is described by

$$V = DH\left(\frac{W_a + W_c}{2}\right) \quad , \qquad (3)$$

and the fraction of gamma ray interactions occurring in the interaction region is approximated by

$$F_i \approx \frac{\left(W_c + W_p\right)\left(2L_i + L_p\right)}{2\left(W_a + W_c\right)\left(L_i + L_p + L_m\right)} \quad . \qquad (4)$$

Effective Frisch grid screening requires a small grid separation. Hence, W_a = 2 mm is imposed in the following examples. With W_c = 10mm, D = 10mm, H = 10 mm, θ = 43.5° and with the Frisch grid = 1 mm wide centered 2.0 mm back from the anode, the fraction of events occurring in the interaction region can be shown to be 85.3%. By comparison, a 2mm thick parallelepiped that is 10mm long and 10mm wide with a 1mm wide Frisch grid centered 2mm back from the anode has F_i = 80%. The fraction of gamma ray interactions occurring in the interaction region is increased for the trapezoidal case over the parallelepiped case, which reduces spectral energy resolution degradation from gamma ray interactions in the measurement region [17]. The general trend for F_i is to approach unity for both designs until the Frisch grid ultimately contacts the anode. Furthermore, the volume of the parallelepiped design is 200 mm^3, whereas the volume of the trapezoid design is be 600 mm^3. The overall result is a 3.2 times increase in detector gamma ray sensitivity in the interaction region for the trapezoidal design, while retaining both effective Frisch grid screening and a higher F_i value.

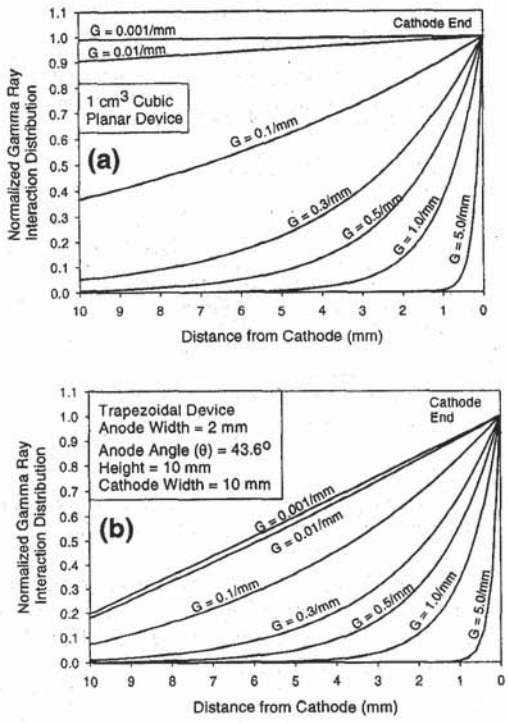

Figure 2. The calculated normalized gamma ray photoelectric probability distribution functions for cathode irradiation of (a) a 1 cm wide planar device and (b) a 1 cm tall trapezoid device. G is the photoelectric linear attenuation coefficient.

The normalized gamma ray probability distribution function is highest near the cathode and lowest near the anode for a trapezoidal shaped semiconductor Frisch grid detector. In the present example (uniform irradiation), the normalized total gamma ray probability distribution function for a trapezoidal device is

$$P_N(x)\,dx = \frac{2x\tan\left(\frac{\theta}{2}\right) + W_a}{H^2\tan\left(\frac{\theta}{2}\right) + HW_a}dx\,, \quad 0 \le x \le H\,, \quad (5)$$

where x refers to the distance from the anode towards the cathode and θ refers to the acute angle at the anode (see Figure 1). Returning to the previous example, consider the number of gamma ray interactions that occur within 1mm of the cathode. Integrating equation 4 from x = 9mm to x = 10mm yields a normalized interaction probability of 16.07%, whereas integrating from x = 0 to x = 1mm yields a normalized gamma ray interaction probability of 3.93%. Statistically over four times as many events will occur within 1mm of the cathode than within 1mm of the anode. The induced charge observed is from charge carrier motion across the device, in which more electron dominated output pulses will be observed than hole dominated output pulses. As a result, the probability of electron dominated induced charge motion is much higher than hole dominated induced charge motion for simple geometric reasons.

2. Effects of Gamma ray attenuation

a. Cathode Irradiation

We now consider the effect of gamma ray attenuation within the material. If irradiated from the cathode end, the overall geometric weighting of electron dominated signals will be more pronounced as the gamma ray energy decreases. To illustrate, the linear gamma ray photoelectric interaction probability for a given differential length is described by

$$F_\gamma = dI(x) = I(x)G\,dx \quad , \quad (6)$$

and the gamma ray attenuation is described by

$$I(x) = I_o e^{-xG} \quad , \quad (7)$$

where I_0 is the gamma ray flux originating from the negative x direction, $I(x)$ is the transmitted gamma ray flux beyond distance x, and G is the gamma ray linear attenuation coefficient for the *photoelectric effect*. The gamma ray interaction rate per differential volume will be greater at the cathode end than at the anode end. Shown in Figures 2a and 2b are the calculated gamma ray interaction probability distributions for planar devices and trapezoidal devices when irradiated from the cathode. For the example, the trapezoid device has the same dimensions as in the previous examples, and the planar device is 1 cm^3. Referring to Figure 2a, the expected gamma ray interaction distribution is fairly uniform for gamma ray energies with normalized photoelectric linear attenuation coefficients (G) less than 0.01. However for G > 0.01, the effect of gamma ray attenuation skews the normalized gamma ray interaction probability distribution such that it increases towards the cathode. For G > 0.1, an energy dependent "pseudo-peak" will form due to the gamma ray interaction probability being greatest near the cathode. Low energy gamma rays will appear in a pulse height spectrum as energy peaks, but high energy gamma rays will appear as small poorly resolved peaks with long "tails." Such is the case observed for CdZnTe planar designed gamma ray detectors [25,26].

Referring to the trapezoidal case shown in Figure 2b, it becomes important to note that the geometric weighting couples with the gamma ray attenuation to further enhance the formation of energy dependent pseudo-peaks in the pulse height spectrum. Notice that only slight differences are discernable between the normalized gamma ray probability distribution functions for the case in which G ≥ 5.0 (Figures 2a and 2b). For the trapezoid prism the geometric weighting effect remains dominant for G < 0.3. The gamma ray interaction probability is significantly larger near the cathode for the geometrically weighted cases, which works to reduce the effects of hole trapping. Hence, an energy dependent "pseudo - peak" that is characteristic of both the detector

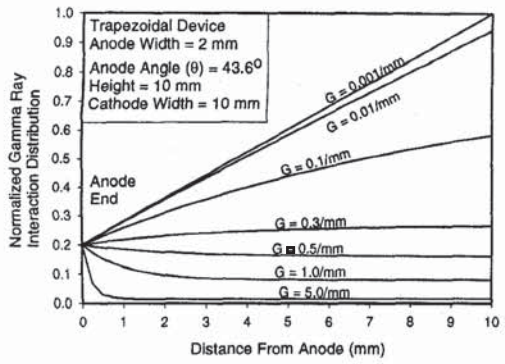

Figure 3. Shown are the calculated normalized gamma ray photoelectric probability distribution functions for anode irradiation of a 1cm tall trapezoid device. G is the gamma ray photoelectric linear attenuation coefficient.

geometric shape and gamma ray attenuation in the device will appear in the pulse height spectrum.

b. Anode Irradiation

Anode irradiation of compound semiconductor radiation detectors generally renders inferior spectroscopic performance to that of cathode irradiation. The highest gamma ray interaction probability will occur nearest the anode, the effect being less important as the value of G decreases (see Figure 3). Assuming a uniform and collimated source, Figure 4 shows conceptually the gamma ray interaction distribution for cathode and anode irradiation for trapezoidal devices. If the device is separated into discrete regions of gamma ray absorption for any value of G, the attenuation of gamma rays from the cathode end decreases in the negative x direction uniformly over the yz plane (Figure 4a). However, if the device is irradiated from the anode end (Figure 4b), the entire upper surface area of the device is exposed to the gamma ray flux, and the normalized gamma ray interaction probability as a function of interaction depth is quite different than the cathode irradiation case. Gamma ray self-attenuation serves to redistribute the normalized interaction probability throughout the device, and the gamma ray absorption is dependent on the x,y and z directions. Cathode irradiation with high values of G confines gamma ray interactions near the cathode region. Anode irradiation with high values of G confine gamma ray interactions primarily over the entire upper surface region of the device.

The normalized gamma ray probability distributions for anode irradiation of a planar device are simply the reverse of Figure 2a. As a result, the majority of observed pulses are dominated by the hole transport properties. Figure 3 shows the calculated normalized gamma ray probability distributions for anode irradiation of a trapezoidal prism device. The distribution demonstrates the appearance of a pseudo-peak for G values less than 0.1/mm. However, the distribution reduces and actually tends towards a constant value as the value of G is increased. The result is a consequence of confining the gamma ray absorption over the surface region of the device. As G increases, the location of the highest gamma ray interaction density is at the surface area of the anode, and the interaction distribution approaches

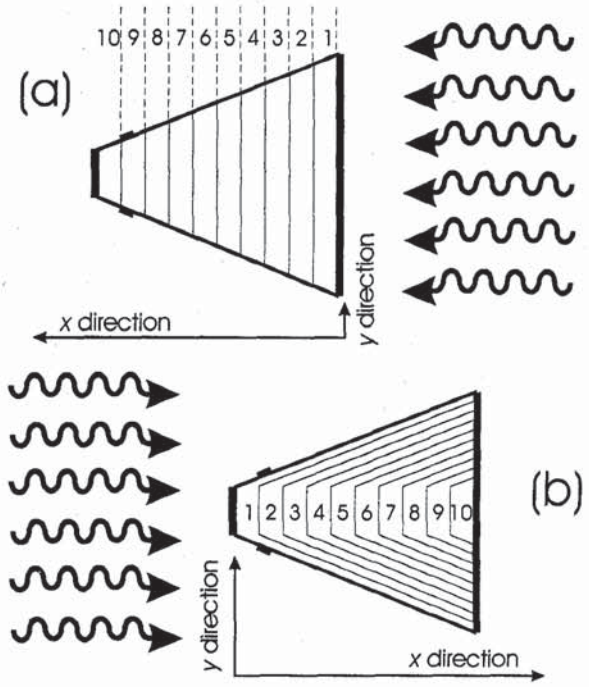

Figure 4. Conceptual diagrams showing regions of similar gamma ray absorption in a trapezoid detector for (a) cathode irradiation and (b) anode irradiation. The cases shown are for mono-direction and collimated gamma ray sources.

a constant value over the remaining range of x in the detector. The result indicates that anode irradiation with low energy gamma rays reduces the effectiveness of geometrical weighting in the device. Proper shielding should be considered such that the probability of anode irradiation is limited.

Overall, the geometric weighting effect is most pronounced for cathode irradiation of the device. The two main effects that arise from geometric weighting are (a) electron dominated transport statistics and (b) increased interaction region to measurement region volume ratio (V_i /V_m). Other shapes will demonstrate similar effects, such as pyramid frustums, conical frustums and hemispheres [9,10].

B. *The Small Pixel Effect*

The induced current and integrated induced charge signal formed from charges moving between two conducting plates was derived by Shockley [27] and Ramo [28], and later shown to apply to planar configuration semiconductor radiation detectors [29,30]. In general, the induced charge from charge carrier motion in the absence of trapping is

$$\Delta Q^* = Q_o \frac{|\Delta x_e| + |\Delta x_h|}{W_D} \quad , \qquad (8)$$

where the electron and hole charge carriers are moving in opposite directions. Such a relationship is not true when the contacts of a device differ in area, a condition referred to as the "small pixel effect" [31].

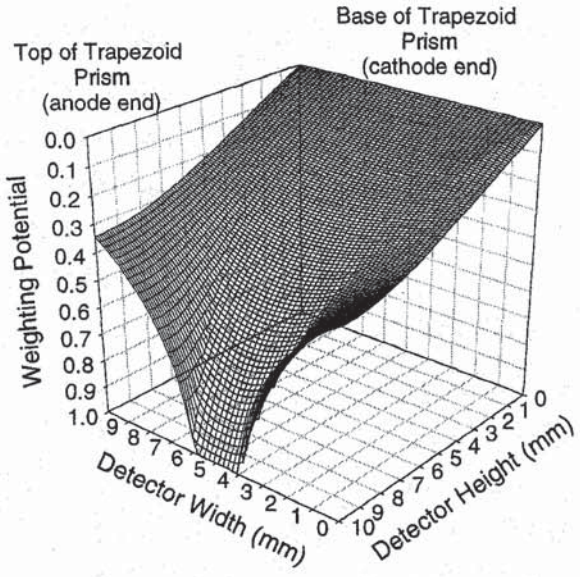

Figure 5. The calculated weighting potential of a trapezoid prism detector. Dimensions are Wa = 2mm, Wc = 10mm and H = 10mm. The charge induction is greatest in the region near the anode.

The "weighting potential" concept is often used to determine the dependence of the observed (or measured) induced charge on the geometry and electrode configuration of a detector [32,33]. In a given environment in which N number of electrodes in a space are connected to ground, the general expression derived by Shockley [27] for the current induced on an electrode by a moving point charge is

$$I_{N=1} = \frac{dq_1}{dt} = -\nabla V_1(r) \cdot \frac{dr}{dt} = E_1(r) \cdot v \quad , \quad (9)$$

where $E_i(r)$ is the electric field at point r due to a *unit* potential on conductor 1 with all others (2 .... N) grounded (set at 0), v is the carrier velocity, and V_i is the potential at conductor 1. The solution to the gradient of $V_i(r)$ with the potential at electrode $N = i$ held at unity (unit = 1.0) and all other conductors held at 0 is the normalized potential distribution or *weighting potential* for charge induction on contact $N = i$. The change in the weighting potential over Δx is equivalent to the change in normalized induced charge $(\Delta Q^*/Q_o)$ for charge carriers moving through the same distance Δx. Solutions for non-symmetric electrode cases can be solved numerically.

In the case that a detector has a small anode and a large cathode, the weighting potential changes much more abruptly near the anode than the region near the cathode. As a result, more charge is induced as charge carriers move in the vicinity of the small anode than charge carriers moving in the vicinity near the cathode. From geometric weighting with the trapezoid prism design, more charge carrier pairs are produced near the cathode over that of the anode. As a result, more electrons will be drifted towards the small anode over the number of holes "born" at the anode. The induced charge

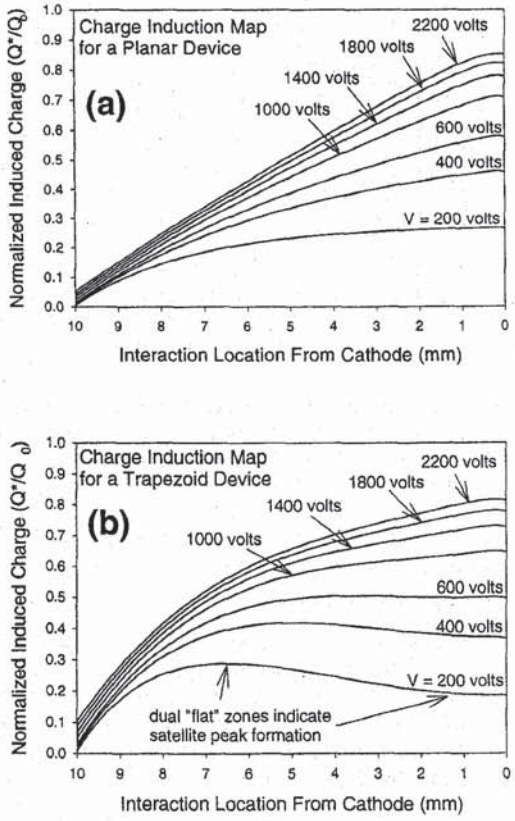

Figure 6. The calculated charge induction maps for (a) a 10mm wide CdZnTe planar detector and (b) a 10mm high trapezoid prism CdZnTe detector. A distance of 10mm separates the anode from the cathode in both cases.

influenced by the electron carriers becomes even greater when the small pixel effect is coupled to the geometrical weighting effect. Figure 5 shows the calculated weighting potential of a trapezoid prism device with the dimensions described in Section II-A. As can be seen, the change in induced charge is greatest in the region near the anode. Hence, electron dominated pulses will result without even having a Frisch grid on the device!

Figures 6a and 6b show a comparison between the charge induction maps [5] of a 10 mm wide planar CdZnTe detector and that of a 10 mm high CdZnTe trapezoid prism device. It was assumed in the calculations that gamma ray irradiation was uniform. Equation 1 was used to calculate the planar case. The trapezoid prism case was determined by convolving the charge carrier trapping and velocity characteristics with the weighting potential, and then numerically calculating the resulting induction map. Typically quoted material properties of CdZnTe were used for the calculations [3]. Flat regions in a charge induction map translate into energy peaks in the pulse height spectrum, and sloped regions in the charge induction map translate into "tail" regions. As can be seen, the trapezoid prism has a much larger flat region than the planar device, indicating tail suppression and more efficient photopeak formation.

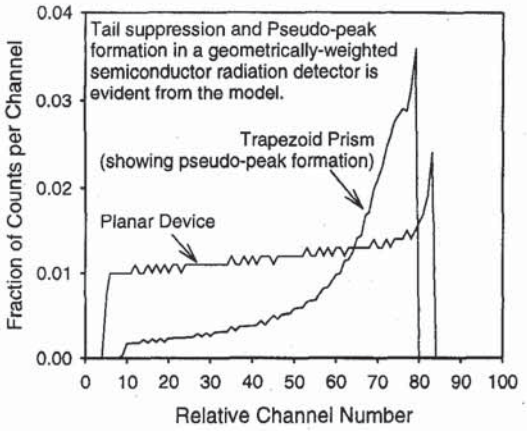

Figure 7. Modeled results of the expected photoelectric pulse height spectrum from a CdZnTe planar detector and a CdZnTe trapezoid prism detector. The distance between the cathode and anode is 10mm in both cases.

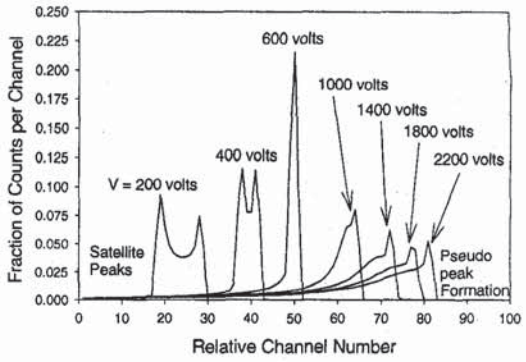

Figure 8. The modeled photoelectric pulse height spectrum progression as a function of bias voltage for a CdZnTe trapezoid prism detector. The distance between the cathode and anode is 10mm. Notice the formation of satellite peaks at low voltages and a pseudo-peak at high voltages.

Figure 7 shows a comparison of simulated gamma ray spectra from a CdZnTe planar device and a CdZnTe trapezoid device. Uniform irradiation was assumed and the calculation was performed for only photoelectric interactions. Typical materials properties were used for the calculation [3]. The "tail" is significantly suppressed in the trapezoid device, and a "pseudo-peak" forms as a natural consequence of the coupling between geometrical weighting and the small pixel effect. Progression of pseudo-peak formation from a trapezoid prism device is modeled and shown in Figure 8. Shown is the expected spectral dependence as a function of increasing bias voltage across the trapezoid device for photoelectric absorptions. Compton scattering and gamma ray attenuation were not considered in the calculation. Notice that the model predicts the formation of "dual peaking" or "satellite" peaks at low voltages. This can be recognized as a direct consequence of the unusual charge induction dependence shown in Figure 6b, in which there are two flat regions appearing in the charge induction map for low applied voltages. As the voltage is increased, the resolution begins to get much better. At higher voltages, the resolution degrades and a full "pseudo-peak" forms. The resulting spectra shows significant tail suppression and the "pseudo-peak" forms near the location expected for the actual gamma ray full energy peak.

C. *The Frisch Grid Effect*

A Frisch grid gas ion chamber is designed to measure the induced charge primarily from electrons in order to compensate for slow positive ion motion [18-20]. The technique involves separating the radiation detector into two regions by a screen or grid. One region is large in volume and is where the majority of gamma ray interactions occur in the device. The other region is small, and is where the induced charge is measured in the device.

A gamma ray interaction occurring in the main volume of the detector excites electron-ion pairs. An externally applied electric field drifts the excited charge carriers in opposite directions, in which the electrons drift through the grid and into the measurement region of the device. The positive ions drift away from the grid and do not enter into the smaller measurement region of the device. From the Shockley-Ramo theorem, the induced charge produced at the anode results from charge carriers moving between the conductive grid and the anode and *not* from charge motion between the cathode and the grid. As a result, the detector is primarily sensitive to only the electron charge carriers. Usually, the measurement region is well shielded such that relatively few gamma ray interactions occur in the measurement region, hence almost all of the measured induced charge is from electrons that have been swept into the measurement region from the interaction region.

The semiconductor counterpart of the gas ion chamber Frisch grid detector operates similarly with these noted differences:

i. The semiconductor Frisch grid detector is used to compensate trapping effects of hole charge carriers, not just for slow rise times from poor charge carrier mobilities.

ii. The semiconductor Frisch grid detector actually has three regions (not two), those being (a) the interaction region, (b) the pervious region and (c) the measurement region (see Figure 1).

iii. The semiconductor Frisch grid detector will still suffer from electron charge loss due to trapping in the interaction, pervious and measurement regions.

iv. The semiconductor Frisch grid detector will most likely be smaller than the Frisch grid ion chamber, hence shielding the measurement region is difficult. As a result, gamma ray interactions will occur in all three regions, and some of the induced charge in the measurement region will be from hole motion originating in the measurement region. Geometrical weighting works to reduce this problem.

Ultimately, the highest spectroscopic performance is achieved with the Frisch grid turned on (grounded). Figure 9 shows the calculated weighting potential of a trapezoid prism

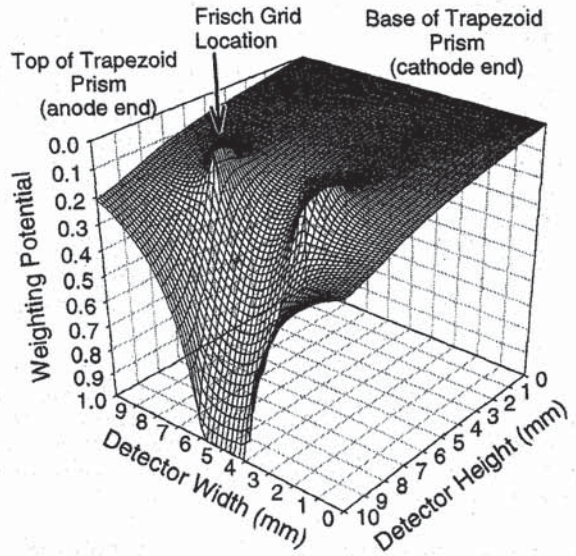

Figure 9. The calculated weighting potential of a trapezoid prism geometrically weighted Frisch grid detector with the Frisch grid connected. Dimensions are Wa = 2mm, Wc = 10mm, Lm = 1.5mm, Lp = 1mm, Li = 7.5mm, and H = 10mm. It is clear that the charge induction is greatest in the measurement region.

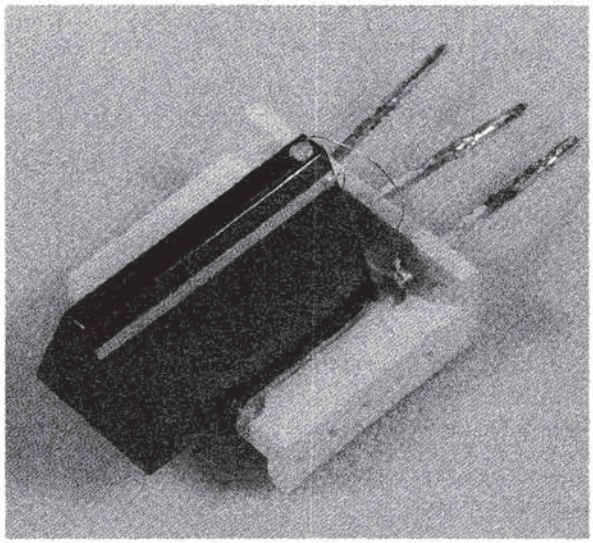

Figure 10. A geometrically weighted Frisch grid trapezoid prism radiation detector fabricated from CdZnTe material. The device volume is 1 cm^3.

Frisch grid radiation spectrometer with the Frisch grid turned on. Clearly, the outstanding screening for such a device is evident in which most of the induced charge measured at the anode will be resultant from charge carrier motion in the measurement region. With the Frisch grid turned on, the device maintains highly effective interaction region screening while maintaining a much larger interaction region than the parallel strip parallelepiped Frisch grid design [16,17,21].

Referring again to Figure 9, it becomes apparent from the gradual change in the weighting potential between the grid and the cathode that some charge is induced on the anode as carriers move through the interaction region. The effect, in part, is a function of the spacing between the Frisch grid strips. Electrons that are excited near the cathode will undergo more trapping as they move to the anode than electrons that are excited near the grid. For mono-energetic gamma ray interactions, electron charge carrier collection improves as interactions occur nearer the grid, yet less charge per electron is induced on the anode than for interactions occurring near the cathode. The effect is fortuitous in that some amount of self-compensation for position dependent charge induction is realized, thereby improving spectroscopic performance.

III. Detector Operation and Experimental Results

Prototype trapezoid prism devices were fabricated and tested at the University of Michigan from "counter grade" CdZnTe material [34]. The devices were designed with 2mm wide anodes and 10mm wide cathodes. The devices were each 10mm tall and 17mm long, giving an overall volume of 1 cm^3. Similar in design to previously reported parallel strip Frisch grid devices [16,17], the Frisch grid strips were centered either 1.5mm or 2mm back from the anode. Figure 10 shows a typical device after fabrication and mounting.

The initial device testing was conducted within an aluminum box with only two connections. The Frisch grid was either "on" (grounded to the box) or "off" (floating). The anode was connected to the input of a commercially available preamplifier (such as an Ortec 142A) and the cathode was connected directly to a high voltage supply. The trapezoid

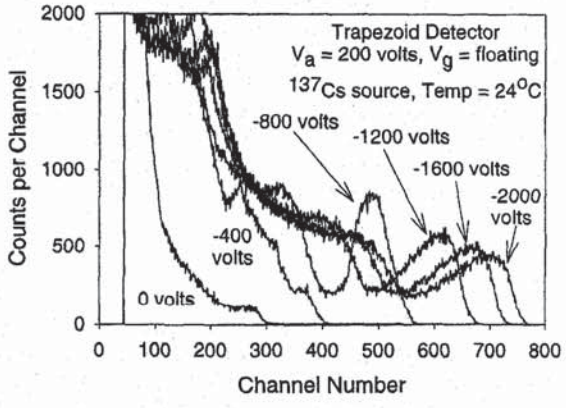

Figure 11. The observed voltage-dependent pulse height spectra of ^{137}Cs 662 keV gamma rays from a CdZnTe trapezoid prism geometrically weighted detector with the Frisch grid disconnected. The distance between the anode and cathode is 10mm. The anode was held at 200 volts and the cathode voltage was changed for the experiment.

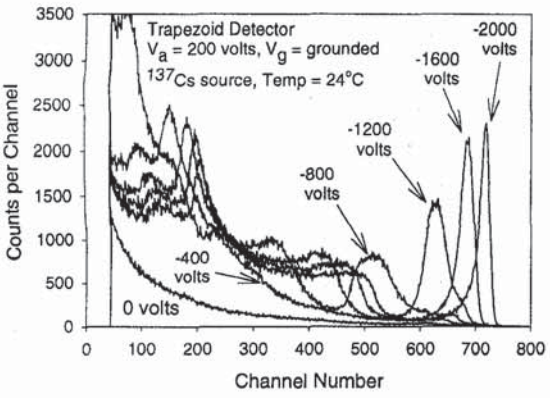

Figure 12. The observed voltage-dependent pulse height spectra of ^{137}Cs 662 keV gamma rays from a CdZnTe trapezoid prism geometrically weighted detector with the Frisch grid connected. The distance between the anode and cathode is 10mm. The anode was held at 200 volts and the cathode voltage was changed for the experiment.

prism devices were first tested with the Frisch grid disconnected in order to observe the coupling of geometrical weighting with the small pixel effect. Shown in Figure 11 is the progression of voltage dependent pulse height spectra as measured from a 10mm tall trapezoid prism detector operated at room temperature (24°C). The anode was biased at 200 volts and the cathode voltage was increased during the experiment. Gamma ray irradiation was performed from the cathode end. The device exhibited the salient features predicted from the modeled response (Figure 8), those being satellite peaks and a pseudo-peak characteristic of the device shape. Hence, it becomes clear that the small pixel effect and the geometrical weighting are affecting the device performance. Although lacking in energy resolution performance, the device outperforms planar structures of similar volume. The performance of the same device was then tested with the Frisch grid grounded to the aluminum box. The anode was biased at 200 volts and the cathode voltage was increased during the experiment. The device was again irradiated with ^{137}Cs 662 keV gamma rays from the cathode end. Figure 12 shows the room temperature (24°C) spectral performance of the device as a function of increasing cathode voltage, in which dramatic improvement in the energy resolution is apparent.

A CdZnTe 1 cm^3 geometrically weighted trapezoid prism detector was tested for ambient temperature gamma ray energy resolution. The device Frisch grid was either floating (off) or grounded (on). In all cases, the anode was held at 200 volts and the cathode was held at negative 2000 volts. The device was operated under ambient room temperature (ranging between 19°C to 29°C) with a commercially available Ortec 142A preamplifier. No pulse selection or correction was used, and the device was not cooled by any means. All irradiation was performed from the cathode end.

Figure 13 shows comparison spectra of 122 keV ^{57}Co gamma rays with the Frisch grid off and on. Although 122 keV gamma rays are mostly absorbed near the cathode (in which case planar detectors can show acceptable energy resolution), improvement can still be seen with the Frisch grid connected. Notice that the 136 keV peak is not resolved until the Frisch grid is turned on. The difference in resolution is much more dramatic for higher energy gamma rays. Figure 14 shows comparison spectra of 662 keV gamma rays with the Frisch grid on and off. Notice the formation of a pseudo-peak when the Frisch grid is floating. Additionally, the energy resolution outperforms ordinary planar CdZnTe detectors of smaller or similar size [25,26], resultant from the coupling of geometric weighting and the small pixel effect. The energy resolution is dramatically improved when the Frisch grid is turned on, demonstrating the advantage of utilizing the three effects together. The device demonstrated 2.68% FWHM

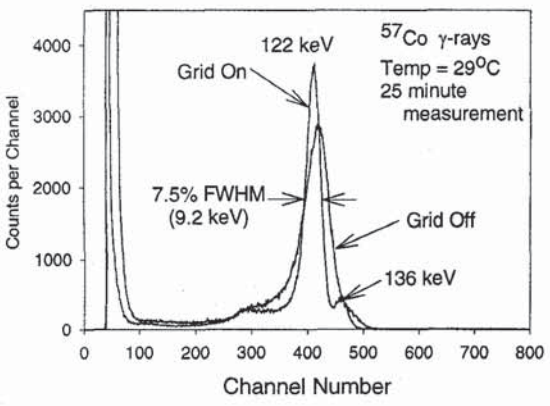

Figure 13. A comparison of ^{57}Co 122 keV gamma ray spectra measured from a 1 cm^3 trapezoid prism detector with the Frisch grid turned off and on.

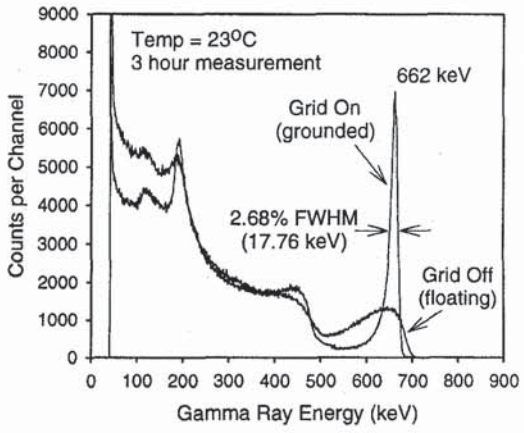

Figure 14. A comparison of ^{137}Cs 662 keV gamma ray spectra measured from a 1 cm^3 trapezoid prism detector with the Frisch grid turned off and on.

energy resolution for ^{137}Cs 662 keV gamma rays. The calculated intrinsic peak efficiency (number of counts in the peak divided by the number of gamma rays intersecting the device plane) at 662 keV is 2.56%.

The device gamma ray absorption efficiency was investigated by comparing its performance to that of a 2"x2" NaI(Tl) detector. A mixed gamma ray calibration standard was used for the measurement, and the source was located approximately at the same distance from either detector during the measurements. At all energies, the CdZnTe trapezoid prism detector outperformed the NaI(Tl) detector regarding energy resolution (Figure 15). At high energies (above approximately 300 keV), the NaI(Tl) detector was clearly more efficient. However, for energies below 300 keV the 1 cm^3 CdZnTe trapezoid prism detector appears to be more efficient. The unexpected result can be attributed to the loss of low energy gamma rays through absorption in the NaI(Tl) detector package. CdZnTe devices need only to be in an electromagnetically shielded light tight container, and do need not be encapsulated in a water tight hermetically sealed reflecting package as do NaI(Tl) detectors. Hence, it is possible that these relatively large CdZnTe devices can be made to outperform modest sized NaI(Tl) devices at low gamma ray energies.

IV. Conclusions

Room temperature operated 1 cm^3 CdZnTe geometrically weighted trapezoid prism Frisch grid radiation spectrometers have been designed and tested. High resolution is achieved without electronic pulse rejection, compensation or correction techniques. The device operates with standard NIM electronics and a standard charge sensitive preamplifier attached directly to the detector anode. The device dimensions have not been optimized yet, indicating that further improvements in detector performance may be achievable. Presently, 2.67% FWHM energy resolution at 662 keV has been achieved with a 1 cm^3 device. By comparison, a 1 cm^3 coplanar grid device had a reported uncorrected energy resolution of 2.4% FWHM at 662 keV [35], and a considerably smaller 27 mm^3 drift diode detector had a reported energy resolution of 5.8% FWHM at 662 keV [15]. The trapezoid device demonstrated relatively high energy resolution at room temperature, and had comparable photo-peak efficiency to that of a standard 2"x2" NaI(Tl) detector at low energies. The applications for such a detector include remote radiation spectroscopy measurements, non-proliferation monitoring and test ban treaty monitoring. Figure 16 shows a room temperature measurement (19°C) of enriched ^{235}U, in which characteristic gamma ray energies are clearly apparent. The device is very simple to operate and requires only one output to a single preamplifier. Presently the devices are operated with two power supplies, however it is expected that a simple resistive divider can be used to operate the device with only one power supply. Hence, a hand held instrument can be realized with relatively simple electronics. In the case that higher resolution is required, compensation electronics similar to those used with co-planar grid devices can be implemented [13]. Further research is presently being conducted to optimize the geometrical design as well as research on schemes to increase the overall volume by arranging the devices in a coaxial array.

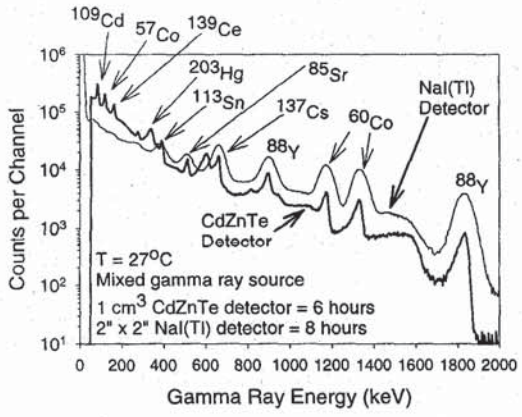

Figure 15. Comparison room temperature gamma ray spectra of a 1 cm^3 CdZnTe trapezoid prism device and a 2 x 2 NaI(Tl) detector. The source distance from the detector was similar in both cases. Note that the count scale is logarithmic.

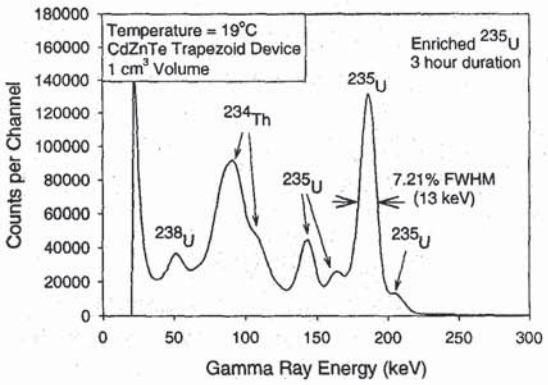

Figure 16. Room temperature gamma ray spectra of enriched ^{235}U emissions measured from a 1 cm^3 trapezoid prism detector.

V. References

[1] E. Sakai, Nucl. Instr. and Meth., "Present Status of Room Temperature Semiconductor Detectors," Vol. 196, 1982, pp. 121-130.

[2] M. Cuzin, "Some New Developments in the Field of High Atomic Number Materials," Nucl. Instr. and Meth., Vol. A253, 1987, pp. 407-417.

[3] D.S. McGregor and H. Hermon, "Room Temperature Compound Semiconductor Radiation Detectors," Nucl. Inst. and Meth., Vol. A395, pp. 101-124, 1997.

[4] R.B. Day, G. Dearnaley, and J.M. Palms, "Noise, Trapping and Energy Resolution in Semiconductor Gamma-Ray Spectrometers," IEEE Trans. Nucl. Sci., Vol. NS-14, pp. 487-491, 1967.

[5] G.F. Knoll and D.S. McGregor, "Fundamentals of Semiconductor Detectors for Ionizing Radiation," Proc. MRS, Vol. 302, pp. 3-17, 1993.

[6] L.T. Jones and P.B. Woollam, "Resolution Improvement in CdTe Gamma Detectors Using Pulse-Shape Discrimination," Nucl. Instr. and Meth., Vol. 124, pp. 591-595, 1975.

[7] M. Richter and P. Siffert, "High Resolution Gamma Ray Spectroscopy with CdTe Detector Systems," Nucl. Instr. and Meth., Vol. A322, pp. 529-537, 1992.

[8] Y. Eisen and Y. Horovitz, "Correction of Incomplete Charge Collection in CdTe Detectors," Nucl Instr. and Meth., Vol. A353, pp. 60-66, 1994.

[9] K. Zanio, Semiconductors for Room Temperature Nuclear Detector Applications, in Semiconductors and Semimetals, Vol. 13, R.K. Willardson and A.C. Beer, Series Eds., Academic Press: New York, 1978.

[10] H.L. Malm, C. Canali, J. W. Mayer, M-A Nicolet, K.R. Zanio, and W. Akutagawa, "Gamma-Ray Spectroscopy with Single-Carrier Collection in High-Resistivity Semiconductors," Appl. Phys. Lett., pp. 344-346, 1975.

[11] P.N. Luke, "Single-Polarity Charge Sensing in Ionization Detectors using Coplanar Electrodes," Appl. Phys. Lett., Vol. 65, pp. 2884-2886, 1994.

[12] P.N. Luke, "Unipolar Charge Sensing with Coplanar Electrodes – Application to Semiconductor Detectors," IEEE Trans. Nucl. Sci., Vol. NS-42, pp. 207-213, 1995.

[13] Z. He, G.F. Knoll, D.K. Wehe, R. Rojeski, C.H. Mastrangelo, M. Hammig, C. Barrett, and A. Uritani, "1-D Position Sensitive Single Carrier Semiconductor Detectors," Nucl. Instr. and Meth., Vol. A 380, pp. 228-231, 1996.

[14] B.E. Patt, J.S. Iwanczyk, G. Vilkelis and Y. Wang, "New Gamma-Ray Detector Structures for Electron Only Charge Carrier Collection Utilizing High-Z Compound Semiconductors," Nucl. Instr. and Meth., Vol. A380, pp. 276-281, 1996.

[15] J.F. Butler, "Novel Electrode Design for Single-Carrier Charge Collection in Semiconductor Nuclear Radiation Detectors," Nucl. Instr. and Meth., Vol. A396, pp. 427-430, 1997.

[16] D.S. McGregor, Z. He, H.A. Seifert, D.K. Wehe and R.A. Rojeski, "Single Charge Carrier Type Sensing with a Parallel Strip Pseudo-Frisch-Grid CdZnTe Semiconductor Radiation Detector," Appl. Phys. Lett., Vol. 72, pp. 792-794, 1998.

[17] D.S. McGregor, Z. He, H.A. Seifert, R.A. Rojeski and D.K. Wehe, "CdZnTe Semiconductor Parallel Strip Frisch Grid Radiation Detectors," IEEE Trans. Nucl. Sci., Vol. NS-45, pp. 443-449, 1998.

[18] O. Frisch, British Atomic Energy Report, BR-49 (1944).

[19] O. Bunemann, T.E. Cranshaw and J.A. Harvey, "Design of Grid Ionization Chambers," Can. J. Res., Vol. A27, pp. 191-206, 1949.

[20] G.F. Knoll, Radiation Detection and Measurement, 2nd Ed., Wiley: New York, 1989.

[21] D.S. McGregor, R.A. Rojeski, Z. He, D.K. Wehe, M. Driver, and M. Blakely, "Geometrically Weighted Semiconductor Frisch Grid Radiation Spectrometers," Nucl. Instr. and Meth., Vol. A422, pp. 164-168, 1999.

[22] W. Aukutagawa and K. Zanio, "Gamma Response of Semi-Insulating Material in the Presence of Trapping and Detrapping," J. Appl. Phys., Vol. 40, pp. 3838-3854, 1969.

[23] N.B. Strokan, V.K. Yeryomin, S.A. Lomashevich, N.I. Tisnek, "Final Results on the Nature of the Pulse-Height Spectrum from Semiconductor Detectors," IEEE Trans. Nucl. Sci., Vol. NS-19, pp. 365-379, 1972.

[24] S.M. Sze, Physics of Semiconductor Devices, 2nd Ed., Wiley: New York, 1981.

[25] J.F. Butler, F.P. Doty, C. Lingren and B. Apotovsky, "Cadmium Zinc Telluride Detectors for Industrial Radiation Measurement," Appl. Radiat. Isot., Vol. 44, pp. 1359-1366, 1993.

[26] A. Parsons, C.M. Stahle, C.M. Lisse, S. Babu, N. Gehrels, B.J. Teegarden and P. Shu, "Room Temperature Semiconductor Detectors for Hard X-Ray Astrophysics," Proc. SPIE, Vol. 2305, pp. 121-132, 1994.

[27] W. Shockley, "Currents to Conductors Induced by a Moving Point Charge," J. Appl. Phys., Vol. 9, pp. 635-636, 1938.

[28] S. Ramo, "Currents Induced by Electron Motion," Proc. IRE, Vol. 27, pp. 584-585, 1939.

[29] G. Cavelleri, G. Fabri, E. Gatti, and V. Svelto, "On the Induced Charge in Semiconductor Detectors," Nucl. Instr. and Meth., Vol. 21, pp. 177-178, 1963.

[30] M. Martini and G. Ottaviani, "Ramo's Theorem and the Energy Balance Equations in Evaluating the Current Pulse from Semiconductor Detectors," Nucl. Instr. and Meth., Vol. 67, pp. 177-178, 1969.

[31] H.H. Barrett, J.D. Eskin and H.B. Barber, "Charge Transport in Arrays of Semiconductor Gamma-Ray Detectors," Phys. Rev. Lett., Vol. 75, pp. 156-159, 1995.

[32] G. Cavelleri, G. Fabri, E. Gatti, and V. Svelto, "Extension of Ramo's Theorem as Applied to Induced Charge in Semiconductor Detectors," Nucl. Instr. and Meth., Vol. 92, pp. 137-140, 1971.

[33] V. Radeka, "Low Noise Techniques in Detectors," Ann. Rev. Nucl. Part. Sci., Vol. 38, pp. 217-277, 1988.

[34] The CdZnTe devices were fabricated at the University of Michigan from CdZnTe material acquired from eV Products located in Saxonburg, PA.

[35] P.N. Luke and E.E.Eissler, "Performance of CdZnTe Coplanar-Grid Gamma Ray Detectors," IEEE Trans. Nucl. Sci., Vol. NS-43, pp. 1481-1486, 1996.